Measurement of the cross section for $H+D_2 \rightarrow HD(v'=3,j'=0)+D$ as a function of angle and energy

James D. Ayers, Andrew E. Pomerantz, Félix Fernández-Alonso,[a] Florian Ausfelder, Brian D. Bean,[b] and Richard N. Zare[c]
Department of Chemistry, Stanford University, Stanford, California 94305-5080

(Received 19 May 2003; accepted 5 June 2003)

Scattering of the $HD(v'=3,j'=0)$ product from the $H+D_2$ reaction is measured as a function of angle and collision energy from 1.39 to 1.85 eV. The plot of the cross section vs angle and energy is believed to be the first fully experimental plot of its kind reported for this benchmark reaction. Changes in the differential cross section (DCS) are observed in this collision energy range, including a forward-scattering component that peaks at about 1.64 eV and is a strong function of collision energy. This feature has been assigned to result from a barrier resonance, but its full interpretation is presently unsettled. These changes in the DCS do not manifest themselves as variations in the integral cross section (ICS), which varies less than 25% over the energy range measured. Comparisons of the DCSs and the ICS with quantum mechanical calculations show quantitative agreement, although some aspects of the DCS near 1.54 eV are not fully satisfactory. © *2003 American Institute of Physics.* [DOI: 10.1063/1.1595092]

I. INTRODUCTION

The hydrogen-atom-hydrogen-molecule exchange reaction is the simplest neutral bimolecular reaction. This simplicity lends it to theoretical study, allowing some of the most detailed comparisons of experimental results with exact quantum mechanical calculations. Reviews and references therein provide details of past studies of the reaction,[1,2] which include state-resolved integral cross sections (ICSs) (Refs. 3 and 4) and differential cross sections (DCSs) (Refs. 5–10) for a number of different collision energies and reactive product states. Recent experiments on product state-specific differential cross sections have revealed unexpected forward scattering. Zare and co-workers have observed such scattering in the DCS for $H+D_2 \rightarrow HD(v'=3,j'=0)+D$ at 1.64 eV collision energy.[9] This peak in the forward scattering direction was present to a smaller extent for $HD(v'=3,j'=1)$ products, but it was absent for higher j' states.[5] Most other observations of differential cross sections for the reaction followed a simple model with backscattering into low j' states and sidescattering into higher j' states.[6,11] Other reports of forward scattering come from Yang and co-workers,[10] who were able to see a forward-scattered peak in the differential cross section for the related $H+HD \rightarrow D+H_2$ reaction at a collision energy of 1.200 eV.

Other recent work in the reaction family has focused on the possible roles of resonances in the reaction. Reactive scattering resonances have played an important role in the experimental history of the $H+H_2$ family of reactions.[1] Attempts to see resonances in the ICS in this reaction family have met with little success.[1,4,12] After much experimental and theoretical discussion about the existence of resonances in the state-resolved ICS, Miller and Zhang[13] predicted that dynamical resonances would not be easily detectable in an ICS measurement. Instead, these authors claimed that resonances for the $H+H_2$ family manifest themselves as ridges in a plot of the cross section as a function of angle and energy, which we shall call an $E-\theta$ plot. Adding to the debate, others showed that these ridges could arise from quasiclassical trajectory (QCT) calculations,[14] complicating the interpretation of these ridges as a purely quantum mechanical phenomenon.

The role of resonances in other benchmark reactions has attracted considerable attention. Work on F+HD has produced clear evidence for a scattering resonance.[15] This resonant behavior is observed both as a ridge in the $E-\theta$ plot and as a peak in the ICS. The existence of a peak in the ICS is related to the fact that the resonance energy is lower than the classical barrier so that there is almost no contribution from nonresonant scattering. This behavior is not the case in our high-energy $H+D_2$ measurements.

Recent theoretical work has attempted to explain observed forward scattering in the $H+D_2$ reaction. QCT calculations[9] show evidence for the forward-scattered feature observed by Zare and co-workers but underestimate its size by at least a factor of 3. Time-dependent wave packet calculations by Althorpe *et al.*[16] were able to reproduce this forward-scattered feature and indicated that it appeared 25 fs after the backward-scattered feature. A fully converged time-independent quantum mechanical calculation by Aoiz *et al.*[17] was also able to reproduce the form of the DCS.

Seeking a more detailed understanding of the forward-scattered feature, we have measured both ICSs and DCSs as a function of collision energy. The raw data have already been presented[1,16] for the DCSs. Here, we begin by detailing

[a]Present address: CCLRC Rutherford Appleton Laboratory, Chilton, Didcot, Oxfordshire OX11 OQX, United Kingdom.
[b]Present address: Department of Chemistry, University of Wisconsin, Madison, Wisconsin 53706.
[c]Author to whom correspondence should be addressed.

the experiments done to obtain this DCS data. Then, we present an excitation function for the $H+D_2 \rightarrow HD(v'=3,j'=0)+D$ reaction between 1.49 and 1.85 eV collision energy. Using both data sets, we construct the first experimentally generated $E-\theta$ plot with quantum state-selective resolution for a member of the $H+H_2$ reaction family. Various theoretical views on the nature of forward scattering in this reaction have been proposed in other works,[17–21] and it appears that it is likely caused by a barrier resonance, although no consensus presently exists about the full interpretation of this behavior. Therefore, we concentrate on reporting in detail the experimental measurement of the cross section as a function of angle and collision energy and keep discussion of theoretical interpretations to a minimum.

II. EXPERIMENT

Two distinct studies were undertaken in the construction of the $E-\theta$ plot. First, the DCS was measured as a function of energy. Later, the energy dependence of the ICS was measured, allowing scaling of the DCS to produce an experimental $E-\theta$ plot. The basic approaches are similar for both experiments, although enough differences exist to merit a careful accounting. The DCS measurement will be described first; changes made to the experiment for the ICS are then presented.

A. Measuring the DCS

Differential cross sections are measured using the photoloc technique (*photo*initiated reaction analyzed with the *l*aw of *c*osines).[22] The photoloc technique uses the fact that the speeds of several species taking part in the reaction can be determined using conservation of energy and momentum. The central equation of photoloc relates the lab-frame speed of the products, v_{HD} to the center-of-mass scattering angle θ,

$$v_{HD}^2 = u_{cm}^2 + u_{HD}^2 + 2u_{cm}u_{HD}\cos\theta, \tag{1}$$

where u_{HD} is the center-of-mass speed of the products, and u_{cm} is the speed of the center-of-mass in the lab frame. Because u_{cm} and u_{HD} are known from the kinematics of the photoinitiated reaction, the scattering angle θ can be determined from a measurement of v_{HD}. In more detail, the center-of-mass angular distribution is determined from a measurement of the distribution of lab-frame speeds of the HD product in a particular quantum state. The apparatus used to measure DCSs using this technique has been described in detail previously.[7] Briefly, HBr (Matheson 99.8%) and D_2 (Cambridge Isotope Labs) are combined in a 1:9 ratio in a stainless steel manifold with a Teflon-lined holding tank. The gas mixture is injected into a stainless steel vacuum chamber by a pulsed valve (General Valve Series 9) with a 0.5 mm orifice. The backing pressure of the mixture is approximately 350 Torr. Supersonic expansion conditions cause translational cooling of the reagents to less than 50 K. The nozzle, laser, and detection systems are triggered by a 10 Hz master clock and a series of delay generators (Stanford Research Systems DG535). The reagents enter the center of the extraction region of a Wiley–McLaren time-of-flight (TOF) spectrometer. A 5 ns pulse of light intersects the molecular beam and photolyzes HBr, generating fast H atoms with a well-defined speed and spatial distribution. Properties of the hydrogen atoms generated from photolysis are discussed below. About 15 ns after photolysis initiates reaction, another laser beam ionizes $HD(v'=3,j'=0)$ products using (2+1) REMPI via *Q*-branch members of the $E,F\,^1\Sigma_g^+ - X\,^1\Sigma_g^+(0,3)$ band. Ions are directed toward a multichannel plate detector by a time-of-flight spectrometer operated in Wiley–McLaren space-focusing conditions, allowing the determination of ion velocities. To increase velocity resolution, a 6 mm conical mask (called a core extractor) is placed in front of the detector so that only ions with negligible velocities perpendicular to the TOF axis are observed. This core extraction technique[23] allows easier conversion between velocity data and the DCS, although the signal level is reduced by at least a factor of 10.

The use of an independent, tunable photolysis source is the main update to this experiment from past measurements of DCSs in this laboratory. The second harmonic of an Nd:YAG (Quanta-Ray GCR-5) pumps a dye laser (PDL-3, DCM or SR 640 dye), the output of which is doubled and mixed with the residual fundamental to generate 1–4 mJ of light in the 203–220 nm range (corresponding to collision energies from 1.85 to 1.49 eV, respectively). The beam is focused into the chamber such that the focus is approximately 5 cm before the axis of the TOF instrument. The resulting photolysis beam is about 1 mm in diameter in the reaction region.

Photolysis produces hydrogen atoms with two different speeds; over the collision energy studied, approximately 85% are produced in a fast channel with Br generated in its $^2P_{3/2}$ spin–orbit ground state.[24] The other 15% are generated at a slower speed, corresponding to the $^2P_{1/2}$ spin–orbit excited state of the bromine photofragment. For photolysis wavelengths greater than 212 nm, the slow channel hydrogen atoms do not have enough energy to form $HD(v'=3,j'=0)$ products. Even when $HD(v'=3,j'=0)$ is formed, the corresponding slow channel signal is by comparison small owing to the small number of slow channel hydrogen atoms, the smaller reaction cross sections at these energies, and fewer collisions of reagents arising from the slower speed of the hydrogen atom. The spatial anisotropy of products from the slow channel is also unfavorable for detection with core extraction using photolysis light with a polarization perpendicular to the detection axis, decreasing its contribution further. Table I summarizes the photolysis conditions used in this experiment and the relationships between the two channels. For DCS measurements, the contribution of the slow channel is ignored. Efforts are made to consider the slow channel in the ICS measurement; these are detailed in Sec. III B.

B. Measuring the ICS

The ICS is a measure of the amount of product formed by the reaction at a given collision energy. We can measure the concentration of a species in a small probe volume spectroscopically by recording the area under the Doppler profile of a REMPI line. Understanding the relationship between the concentration of product formed and the cross section as a

TABLE I. Characteristics of reaction as a function of photolysis wavelength. The fast-channel E_{coll} is the collision energy of the primary reaction. Raised dots in the slow-channel E_{coll} column indicate that the channel is energetically inaccessible.

Wavelength (nm)	Fast channel E_{coll} (eV)	Slow channel E_{coll} (eV)	Fast channel H speed (km/s)	Fast channel HD max speed (km/s)	Slow channel contribution (%)
220	1.49	⋯	18.9	5.98	⋯
217.54	1.54	⋯	19.2	6.32	⋯
215.15	1.59	⋯	19.5	6.62	⋯
212.8	1.64	⋯	19.8	6.91	⋯
210	1.70	1.35	20.2	7.24	<1
207.86	1.75	1.39	20.5	7.48	2
205.7	1.80	1.44	20.8	7.72	9
203.5	1.85	1.49	21.1	7.96	13

function of collision energy allows us to construct from experimental data an excitation function, which is the variation of the ICS with collision energy. A simple rate-law analysis[25] allows us to express the measured HD signal in terms of quantities we either know or want

$$n_{HD}(t) = \sigma(E, v', j') v n_H n_{D_2} \cdot t, \tag{2}$$

where n_i is the concentration of species i, v is the relative velocity of the reagents, t is the time between photoinitiating and probing the reaction, and σ is the cross section as a function of energy E, final vibrational state v', and final rotational state j'. This treatment assumes that the concentrations of H and D_2 reactants do not change over the time reaction is allowed to occur, an assumption that is examined and verified experimentally (see flyout, Sec. II D 1).

Determining the cross section as a function of collision energy requires understanding how the various terms in Eq. (2) vary as the energy is changed. The amount of HD generated as a function of collision energy is found spectroscopically using REMPI. The relative velocity is known; it is proportional to the square root of the collision energy. The delay time t is held constant throughout all tests. The only remaining consideration is the variation of reagent concentrations as a function of other experimental parameters.

The concentration of hydrogen atoms depends on both the concentration of HBr precursor and the characteristics of the photolysis source. The large wavelength range needed to access the span of collision energies in this study resulted in significant variation of the photolysis laser beam characteristics. Elements affecting H concentration include amount of HBr in the gas mixture, nozzle pulse reproducibility, photolysis laser power, photolysis mode, HBr absorption cross section, and laser alignment. All these variables can either be controlled or corrected for experimentally, but the corrections are cumbersome and introduce considerable uncertainty. We avoid these problems by directly measuring the H-atom concentration using (2+1) REMPI.[26] Scans over the Doppler profile are power-corrected to determine the hydrogen-atom concentration.

Unlike the hydrogen-atom reagent, n_{D_2} does not depend on laser properties; it is a function only of the properties of the pulsed valve and of the reactive gas mixture. Stabilization of the gas delivery system (and thus the concentration of D_2 reagent) is discussed in the next section. The remaining variable is the nozzle backing pressure. Studies show that over the approximately 20% change in backing pressure incurred during an experimental run, the variation of D_2 can be corrected for.

The ICS is thus proportional to the ratio of the amount of HD product to the amount of H-atom reactant at a given collision energy. Corrections can be made for the nozzle backing pressure, the relative velocity of the reagents, and the power variations of the probe lasers. The cross section is given by

$$\sigma(E) \propto \frac{S_{HD}}{S_H \sqrt{E} \xi(P_{back})}, \tag{3}$$

where S_i is the power-corrected signal of species i as a function of collision energy, and $\xi(P_{back})$ is a correction factor between 0.5 and 1, which corrects for changes in D_2 concentration as a function of backing pressure.

C. Experimental changes for the ICS

Although the main experimental techniques were similar to methods used for the DCS, changes were needed to measure the ICS accurately. One change already mentioned is the need to measure hydrogen-atom concentration. H-atom REMPI detection is accomplished by the frequency-doubled output of a dye laser pumped by the third harmonic of an Nd:YAG laser. Because so little laser light (about 15 μJ/pulse) is needed to effect ionization, laser fluence is measured by recording transmission through a fused silica window using a powermeter (Molectron, EPM 1000 with Jmax25 head). The reflected light is then directed into the vacuum chamber for hydrogen-atom detection. Tests verified that the transmitted light intensity was proportional to the intensity of the beam entering the chamber over the range of laser wavelengths and pulse energies used in the experiment. The experimental setup precludes simultaneous measurements of H and HD. Scanning separately can introduce error because the conditions are not necessarily the same. To minimize this error, HD and H scans are alternated, and a series of scans of similar types are compared to ensure that no changes have occurred in the course of a measurement. In

addition, we check the signal stability over long periods to ensure that drift is minimized (see signal stability verification, Sec. II D 4).

Other changes stem from the fundamental difference between ICS and DCS measurements; measuring the DCS requires velocity-resolved measurement of products, whereas measuring the ICS requires collection of all ions. These goals are somewhat contrary because methods used to maximize velocity resolution often result in a reduction in the fraction of ions collected. Several changes accomplished increased ion collection efficiency. First, the core extractor was removed, allowing ions that would normally be masked due to off-axis velocity to impinge on the detector. Next, the time-of-flight voltages were increased, moving the ions toward the detector faster and not allowing for their dispersion to a size greater than that of the detector (1 in. diam). Even with these changes, some of the fastest-moving H ions had speeds too high in a direction perpendicular to the time-of-flight axis; to detect these ions, an electrostatic lens was added to the time of flight spectrometer. This einzel lens was designed with the ion optics simulation code SIMION (Ref. 27) to focus all of the fastest H atoms to an area of about half the size of the detector. Simulations were done to ensure that all H and HD ions likely to be generated in the experiment would be collected. Experimental tests varying the photolysis laser polarization and changing the ion packet steering confirmed that all ions were collected.

Because the ICS is a measure of the amount of signal, the concentration of reagents must be kept constant. Manifold and nozzle changes provided a more stable reagent supply. The gas delivery system must be passivated carefully for consistent performance. A stainless steel manifold was no longer suitable, so a glass manifold was constructed to hold the reactive mixture. Teflon- and silcosteel-coated tubes (Restek Corp.) were used to make connections between the manifold and gauges, gas cylinders, and the pulsed valve. These materials are more inert to HBr corrosion than uncoated stainless steel. The pulsed valve was electropolished, exposing a highly passivated steel surface to reagents. To ensure thorough mixing of gases, reagent mixtures were prepared and allowed to sit the night before an experiment. When not in use, the manifold was baked at approximately 60 °C and evacuated to pressures less than 10 mTorr.

A more stable light source was also needed. Light at about 225 nm for HD ionization was previously generated using a 1064-nm mixing process in potassium dihydrogen phosphate (KDP) crystals; unfortunately, this process generated only about 1 mJ/pulse of energy, and both the power and spatial mode varied dramatically with small changes in room temperature. A different method of light generation reduced these difficulties. The third harmonic of an Nd:YAG laser (Quanta-Ray GCR-3) is mixed in a β-barium borate (BBO) crystal with the $\approx$613 nm output of a dye laser (Lambda Physik LPD 3000) pumped by the second harmonic of the same YAG. This 355-mixing system generates as much as 10 mJ per pulse. Sensitivity to temperature changes was dramatically decreased by using BBO instead of KDP and by reducing the number of mixing stages outside of a temperature-controlled harmonic generator. Normal operating conditions utilized approximately 3 mJ of power.

Burns on chamber entrance windows also affected light reaching the reaction region, changing both the power and mode in unpredictable ways. The cause of these burns was traced to residual diffusion pump oil in the chamber. Installing two turbomolecular pumps (Varian TV 1001 Navigator) with an oil-free backing pump (Varian TriScroll 600) essentially eliminated this problem.

D. Experimental checks on the ICS

1. Product flyout

Equation (2) shows that the amount of product is expected to increase linearly as a function of time t. A delay that is too long, however, results in substantial loss of products from the probe volume via flyout or collisional relaxation, two processes not included in the derivation of Eq. (2). Collisional relaxation is not an issue for this experiment owing to the low concentrations of molecules in the free-jet expansion and the 15 ns time scale between photoinitating and probing the reaction. Flyout is a concern that introduces a bias against faster-moving products. This effect is especially important because we are trying to measure the total amount of products formed irrespective of their velocity. To measure the onset of flyout, both H and HD signal levels were measured as a function of delay between the firing of the photolysis and the probe lasers for a collision energy of 1.85 eV. For delays between about 5 and 10 ns, the hydrogen-atom concentration was constant, which indicates no measurable flyout. Tests with HD indicate that delays between about 5 and 20 ns are acceptable.

These numbers can be compared with a rough estimate of the flyout time, which is based on experimental parameters. In this experiment, the probe beam size is much smaller than the photolysis beam size, so a characteristic flyout time is the time required by an H atom to travel half the diameter of the photolysis beam. The photolysis beam is about 1 mm in diameter; a fast hydrogen atom traveling 20 km/s (see Table I) can traverse half the beam in 25 ns. Finite photolysis and probe laser time widths, finite probe spot sizes, and imperfect beam modes imply that the actual delay times needed to avoid flyout are shorter than the theoretical 25 ns time, consistent with results of delay studies.

2. Invariance with photolysis beam power and size

During the course of the measurements, the power and size of the photolysis beam can vary due to changes in the characteristics of the dye laser and optical beam train used to generate and transmit light to the experimental region. Scanning the photolysis beam over a 15 nm range in the ultraviolet causes the power of the photolysis beam to vary by a factor of 3. These variations result primarily from changes in the dye gain curve as a function of wavelength. Experimental measures of the rate constant must be invariant with respect to changes in the photolysis pulse power. To test this invariance, laser power was decreased by a factor of 3. The change in measurements of the relative cross section was less than 5%, a variation within our experimental uncertainty. Furthermore, changes in the focusing characteristics of the photoly-

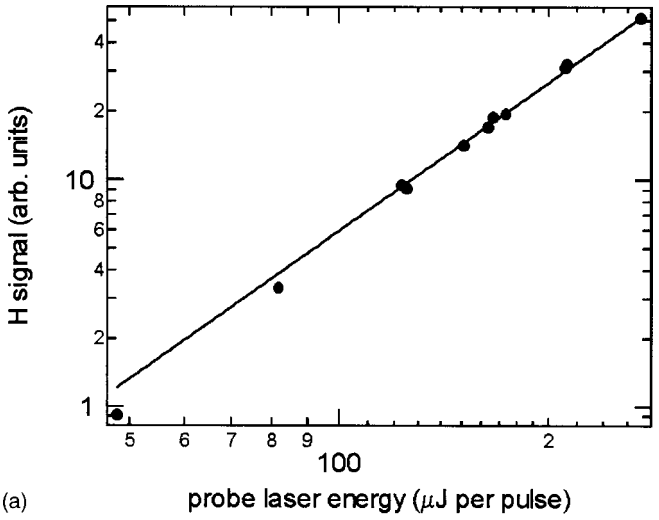

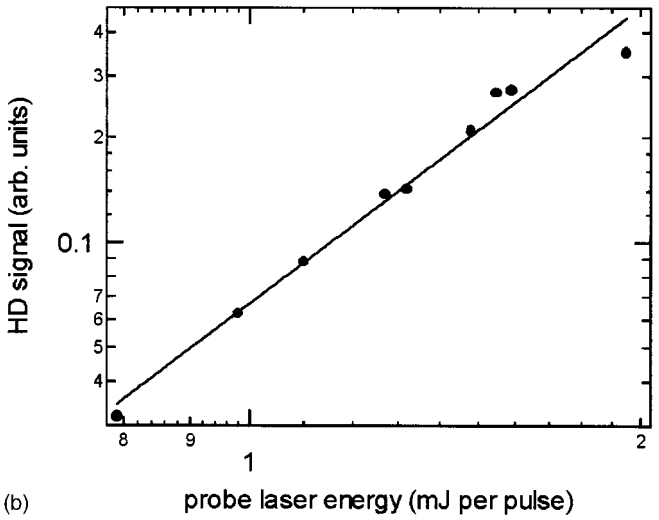

FIG. 1. Log–log plots of the ion signal vs the probe laser power for the (a) H-atom reagent and (b) HD($v'=3,j'=0$) products. The slope of the fit to the data corresponds to the exponent in the power-law associated with the variation of the signal with the laser power.

sis lens as a function of wavelength can affect the photolysis beam size. The photolysis lens is moved as the energy is changed in an attempt to keep the spot size constant throughout the experiment. Even so, the measured rate constant should be insensitive to variations in the size of the photolysis beam, provided it is large enough that flyout is not an issue. To verify this fact, the lens used to focus the photolysis laser was varied over a range of 2.5 cm, modulating the beam size by about 50%. No measurable change in the HD:H signal ratio was detected.

3. Signal variation with probe laser power

Probe light from dye lasers is not stable enough to ignore its contribution to the signal level; over the course of a scan, the power could change by as much as 20%. Relating signal levels to concentration irrespective of probe laser power is essential to measurement of an ICS. The variation of signal level with probe laser power was thus studied. The data are fit to a power law functional form, and exponents derived from these fits are used to correct the signal for variations in the probe laser power. The HD signal was found to vary roughly with the laser fluence to the 2.35 power; the H-atom signal scaled with the fluence to the 2.85 power. Figure 1 shows representative power law plots. The power law exponents are within the 1.5–3 range, which is the expected range for (2+1) REMPI processes where some saturation might occur.[28]

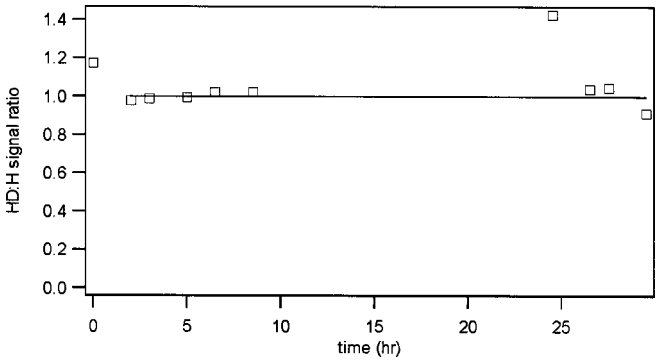

FIG. 2. Measured HD:H signal ratio over a 2 day period. Each square represents one measurement of the ratio; the line is a fit of the data to a straight line. The initial data point of each day does not fall near the line owing to a warm-up period required for signal stability (see text).

4. Signal stability verification

Signal changes over the period of a day from other origins were then considered. Changes could come from sources such as differences in the amount of reagents delivered into the chamber, chemical contamination of the reactive mixture over time, varying detector response, and changing quality of laser and optical systems. To test signal stability, the ICS for the title reaction at 1.85 eV collision energy was measured as a function of time; Fig. 2 shows results from tests on two consecutive days. The measured ICS remains the same over 2 days of testing. The initial measurement on each day gave a high value for the ICS; changes in the first 2 h of running the experiment are attributed to various aspects of reaching steady-state operation. These include imperfect gas mixing in the lines leading to the nozzle and laser warm-up periods. ICS measurements were only trusted after this 2 h warm-up period had passed.

III. RESULTS AND DISCUSSION

A. Differential cross section

Differential cross sections were measured at each of nine collision energies between 1.39 and 1.85 eV. The lowest energy DCS was taken using a single laser both to photolyze HBr and to ionize HD, resulting in $E_{\mathrm{coll}}=1.39$ eV. Low signal at 1.39 eV required 100 000 laser shots to obtain an analyzable time-of-flight (TOF) profile. For all other energies, an independent photolysis source was used. Three trials of 30 000 laser shots each were averaged for analysis. The time-of-flight profiles for both one- and two-laser signals have already been presented.[1,16] The photoloc technique allows conversion of these time-of-flight profiles into DCSs. A photoloc experiment has a one-to-one relationship between the

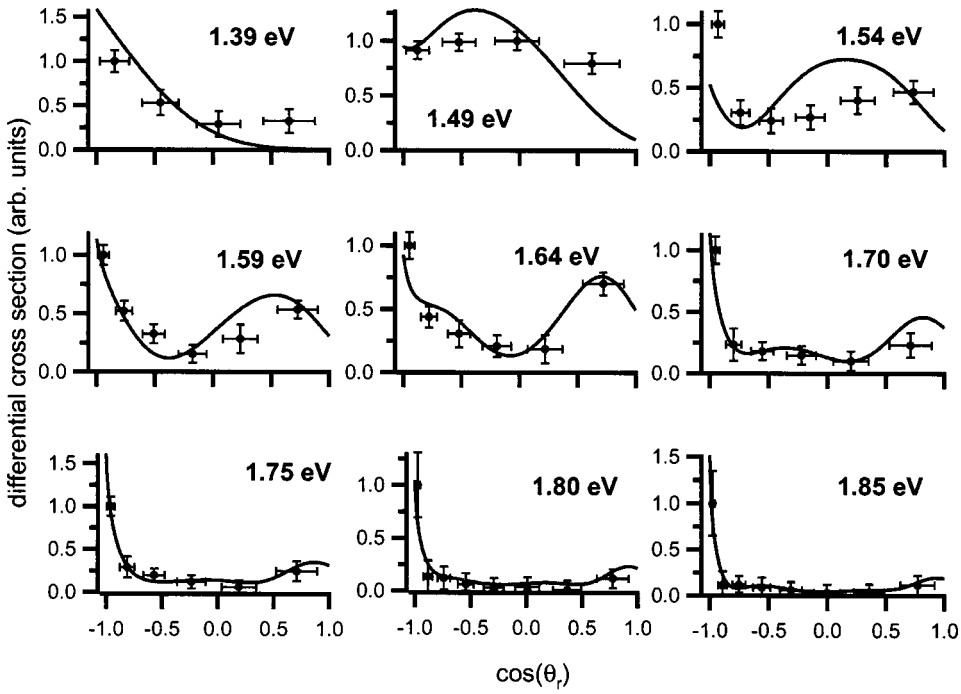

FIG. 3. Differential cross sections for HD($v'=3,j'=0$) products as a function of collision energy. Filled circles with error bars are experimental points; the solid line represents the theory of Althorpe blurred with our experimental instrument function.

lab-frame velocity of the product molecules and the center-of-mass scattering angle given in Eq. (1); this relationship allows extraction of the DCS from a speed-sensitive TOF profile.[22] The TOF data are fit with a number of basis functions that describe the instrumental response as a function of scattering angle. Further details of the algorithms used to convert time-of-flight profiles into differential cross sections are discussed elsewhere.[7] Figure 3 shows the experimental differential cross sections as a function of collision energy (circles with error bars) along with the theory of Althorpe blurred with our experimental resolution function (smooth line). Details of the method used to blur the theory are described below. Causes of experimental blurrings include finite laser pulse duration and finite core-extractor size, which place limits on velocity resolution. Our resolution is roughly constant in velocity space. Because the mapping between scattering angle and product velocity is nonlinear [see Eq. (1)], our resolution is angle-dependent, so that the angular resolution is better in the backward-scattered hemisphere than it is in the forward-scattered hemisphere. The resolution is also affected by the change of lab-frame velocity range caused by a change in the collision energy. This variation results in lower resolution (fewer basis functions used in the fitting) for this particular reaction at the lower collision energies in the study. Fewer experimental points in the low-energy DCSs shown in Fig. 3 are a direct result of this lower resolution.

Theory and experiment are compared by blurring the theoretical DCSs with an instrumental resolution function. DCSs are scaled so that they have the same vertical scale. The blurred theory is obtained by converting a theoretical DCS to an ion velocity distribution, convolving this distribution with a Gaussian functional form approximating experimental resolution, and then converting the blurred velocity distribution back into a DCS. Blurring is particularly important in the forward-scattering direction; experimental angular resolution is quite poor in this direction ($\pm 20°$), and theoretical DCSs show large oscillations with widths of only a few degrees. The result of this blurring is that rapid oscillations in the forward direction are washed out into broad features. In the blurred DCSs, the total amount of product scattered into a large range of angles in the forward direction appears to be integrated and then redistributed in the forward direction. This mimics the blurring observed in the experiment; poor resolution prevents determination of detailed angular information in the forward direction. The basic idea we can extract from the data is the amount of total forward scattered product density. This effect is discussed in more detail in Ref. 14. Another technique, called forward convolution,[25] has been used in the past to compare theory with the results of a photoloc experiment. In this method, theory is used to simulate what would be measured if the theoretical DCS were an accurate depiction of the scattering. This technique has been applied to this data and shown similar results to those obtained with the blurred theory analysis.[16,17] Using either technique, comparison between theory and experiment is excellent at all energies except 1.54 eV. The disagreement at this energy is not well understood, but it is believed that the rapidly changing cross section around 1.54 eV may contribute to this discrepancy.

Cursory examination shows that the amount of forward scatter relative to backward scatter changes sharply as a function of collision energy. The lowest energy point at 1.39 eV is near the energetic threshold (1.32 eV) for the reaction generating HD($v'=3,j'=0$); it shows little forward scatter. At 1.49 eV, the DCS appears isotropic. At higher energies, forward–backward scattering dominates, with forward scattering peaking at about 1.64 eV. The fraction of products that are forward scattered decreases as the energy is increased to 1.85 eV.

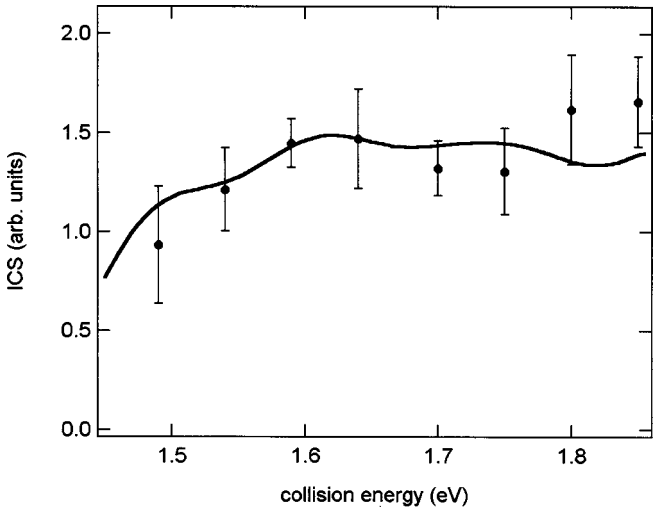

FIG. 4. Integral cross sections for HD($v'=3,j'=0$) product generation between 1.49 and 1.85 eV collision energy. Experimental results are shown as circles with error bars; theoretical calculations of Althorpe are shown as a smooth line. Experimental data have been corrected for slow-channel production, and the theoretical values have been blurred with a 50 meV Gaussian representing the experimental instrument function.

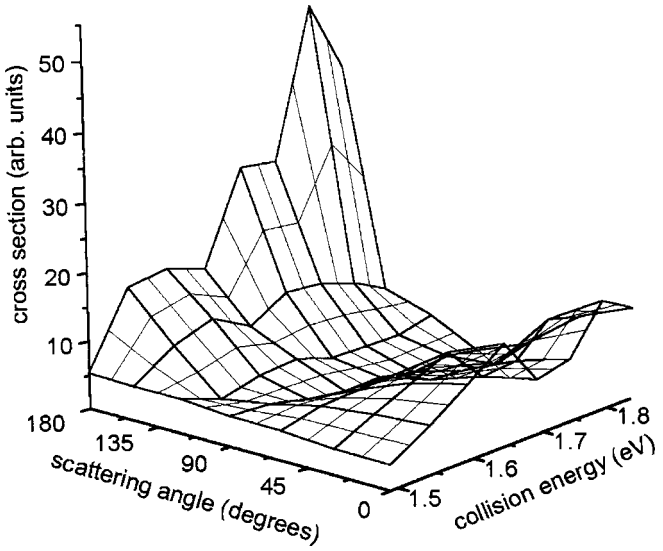

FIG. 5. The cross section is plotted as a function of both collision energy and angle, called an $E-\theta$ plot. A clear peak in the forward scattering direction is seen at 1.64 eV. Changes in the backward to forward scattering with increasing collision energy show the possible appearance of a ridge structure.

B. Integral cross section

The integral cross section was measured at eight different collision energies between 1.49 and 1.85 eV. Three independent measurements were made at each collision energy. Each trial required the experiment to run continuously for approximately 33 h. The Doppler profiles of both HD($v'=3,j'=0$) and H atom REMPI lines were scanned between four and six times at each collision energy. Signal levels were compared to make sure that they did not change from scan to scan. Laser intensity was recorded simultaneously with signal level to allow correction for changes in probe power. The order of energies scanned was varied as a safeguard against experimental drift. The ICS measurement at the first energy studied in a given trial was repeated at the end of the 30 h experimental period; this allowed correction for changes in the backing pressure. The relative cross section was then found using Eq. (3). Laser dye and mirror changes in the photolysis line were necessary to cover the full range of collision energies.

The three independent measurements gave the same integral cross section within statistical error bars. The average is shown in Fig. 4 and listed in Table II. Along with the experimental data, theoretical results from Althorpe[29] are presented. Because our experiment does not measure the absolute cross section, the data are scaled so that the area under the experimental curve is equal to the area under the theoretical curve. Note that energies for the ICSs correspond to those for the DCSs, except for a missing ICS measurement at 1.39 eV. This lowest energy corresponds to the prompt reaction in which the probe laser also acts as the HBr photolysis source. Competition from the one-laser process makes this measurement difficult. At all other energies, the one-laser signal is less than 10% of the total signal.

TABLE II. The cross section for $H+D_2\rightarrow HD(v'=3,j'=0)+D$ as a function of energy.

Energy (eV)	Cross section (arb units)
1.49	0.09
1.54	0.11
1.59	0.13
1.64	0.13
1.70	0.12
1.75	0.12
1.80	0.15
1.85	0.15

The slow channel interferes with measurements at collision energies of 1.70 eV and above. Calculations and experiment can facilitate data interpretation. Small one-laser HD signal indicates low relative cross section at 1.39 eV. Quantum-mechanical (QM) calculations show that the cross section decreases further still at lower energies. At 1.70 and 1.75 eV, these calculations estimate that less than 1% of the reaction signal comes from the slow channel, much smaller than our experimental uncertainty. At higher energies, more of a contribution is expected. The measurement at 1.85 eV collision energy has a contribution from the slow channel reaction at 1.49 eV. Experimental data from 1.85 and 1.49 eV scans indicate a $9\pm4\%$ contribution from slow-channel products. QM calculations[29] taking into account our energy resolution indicate a 13% slow-channel contribution. The same calculations indicate a 9% contribution from slow-channel products at 1.80 eV. Data presented in Fig. 4 and used to create the experimental $E-\theta$ plot include 6% and 9% corrections for the slow channel. Note that these small corrections are within presented statistical error bars.

These data are combined in Fig. 5 to form an $E-\theta$ plot. Each differential cross section is integrated over all angles and scaled so that the area under the graph is equal to the measured cross section. In this plot, a peak in the amount of forward-scattered products at about 1.64 eV is evident. With

such stark changes in the shape of the differential cross section as seen in Fig. 3, it might be expected that the ICS would also change. Both measurements and calculations indicate that over the range studied, no significant changes in the ICS occur. We conclude that the mechanism causing sharp changes in the DCS does not manifest itself as variations in the ICS.

Several groups have made theoretical calculations of this cross section.[17,18,29] A comparison between our experiment and the calculations of Althorpe[29] is shown in Fig. 4. The calculations are convoluted with a 50 meV Gaussian to allow more realistic comparison with our experiment with finite energy resolution. The experiment and theory agree within experimental uncertainty.

The source of the forward scatter and what causes the DCS to change so much with energy is still under debate. Recent ideas about the cause of the forward scattering are discussed by Althorpe and Clary.[30] Work by Althorpe[16,19] shows that the origin of the forward scattering is a time-delayed mechanism. Truhlar and co-workers[21] suggest the existence of a barrier resonance based on a vibrationally adiabatic model. At the same time, Kendrick[18] sees no resonance for the energies and states of this study. Aoiz *et al.*[17] did an analysis that points to the opening of adiabatic thresholds of the transition state as the cause of the forward scattering. Work by Sokolovski furthers the idea that the forward scattering is caused by several poles in the S matrix associated with a barrier.[20] Further work is needed to determine the meaning of the observed forward scattering feature and to understand whether nonadiabatic contributions, such as geometric phase effects, contribute to what is observed. Continued cooperation between experimental and theoretical studies is essential to resolve this issue.

IV. CONCLUSIONS

We have measured the cross section as a function of both energy and angle for the $H+D_2 \rightarrow HD(v'=3,j'=0)+D$ reaction using the photoloc technique. The differential cross section for reaction is found to change dramatically over the 1.39–1.85 eV collision energy range, but the integral cross section shows no significant changes. An important feature in the differential cross section is the relative amount of forward versus backward scattering. The forward-scattering component peaks at around 1.64 eV collision energy. The forward-scattered feature has been shown to be associated with a time delay compared to the back-scattered feature and is suggested to result from a barrier resonance. From the experimentally determined differential and integral cross section data, an $E-\theta$ plot is constructed, which shows hints of a characteristic ridge. Comparisons between experiment and quantum-mechanical calculations that do not include geometric phase effects agree quantitatively, although the DCS measurements near 1.54 eV do not agree with calculations.

ACKNOWLEDGMENTS

The authors would like to thank Stuart Althorpe, Luis Bañares, and Brian Kendrick for providing theoretical results for comparison with experiment. J.D.A. thanks the Fannie and John Hertz Foundation for support in the form of a graduate fellowship. A.E.P. thanks the National Science Foundation for graduate support. The authors are grateful for the continued support of the National Science Foundation.

[1] F. Fernández-Alonso and R. N. Zare, Annu. Rev. Phys. Chem. **53**, 67 (2002).
[2] H. Buchenau, J. P. Toennies, J. Arnold, and J. Wolfrum, Ber. Bunsenges. Phys. Chem. **94**, 1231 (1990).
[3] E. E. Marinero, C. T. Rettner, and R. N. Zare, J. Chem. Phys. **80**, 4142 (1984); R. S. Blake, K.-D. Rinnen, D. A. V. Kliner, and R. N. Zare, Chem. Phys. Lett. **153**, 365 (1988); K.-D. Rinnen, D. A. V. Kliner, R. S. Blake, and R. N. Zare, *ibid.* **153**, 371 (1988); K.-D. Rinnen, D. A. V. Kliner, and R. N. Zare, J. Chem. Phys. **91**, 7514 (1989); D. A. V. Kliner, K.-D. Rinnen, and R. N. Zare, Chem. Phys. Lett. **166**, 107 (1990); D. A. V. Kliner and R. N. Zare, J. Chem. Phys. **92**, 2107 (1990); D. E. Adelman, N. E. Shafer, D. A. V. Kliner, and R. N. Zare, *ibid.* **97**, 7323 (1992); D. Neuhauser, R. S. Judson, D. J. Kouri, D. E. Adelman, N. E. Shafer, D. A. V. Kliner, and R. N. Zare, Science **257**, 519 (1992); D. E. Adelman, H. Xu, and R. N. Zare, Chem. Phys. Lett. **203**, 573 (1993); D. P. Gerrity and J. J. Valentini, J. Chem. Phys. **79**, 5202 (1983); **81**, 1298 (1984); **83**, 2207 (1985); **82**, 1323 (1985); D. K. Veirs, G. M. Rosenblatt, and J. J. Valentini, *ibid.* **83**, 1605 (1985); H. B. Levene, D. L. Phillips, J.-C. Nieh, D. P. Gerrity, and J. J. Valentini, Chem. Phys. Lett. **143**, 317 (1988); D. V. Lanzisera and J. J. Valentini, J. Chem. Phys. **103**, 607 (1995).
[4] J.-C. Nieh and J. J. Valentini, Phys. Rev. Lett. **60**, 519 (1988); D. L. Phillips, H. B. Levene, and J. J. Valentini, J. Chem. Phys. **90**, 1600 (1989); J.-C. Nieh and J. J. Valentini, *ibid.* **92**, 1083 (1990).
[5] B. D. Bean, J. D. Ayers, F. Fernández-Alonso, and R. N. Zare, J. Chem. Phys. **116**, 6634 (2002).
[6] F. Fernández-Alonso, B. D. Bean, and R. N. Zare, J. Chem. Phys. **111**, 1035 (1999).
[7] F. Fernández-Alonso, B. D. Bean, and R. N. Zare, J. Chem. Phys. **111**, 1022 (1999).
[8] F. Fernández-Alonso, B. D. Bean, and R. N. Zare, J. Chem. Phys. **111**, 2490 (1999); L. Schnieder, K. Seekamp-Rahn, E. Wrede, and K. H. Welge, *ibid.* **107**, 6175 (1997).
[9] F. Fernández-Alonso, B. D. Bean, J. D. Ayers, A. E. Pomerantz, R. N. Zare, L. Bañares, and F. J. Aoiz, Angew. Chem., Int. Ed. Engl. **39**, 2748 (2000).
[10] S. A. Harich, D. Dai, C. C. Wang, X. Yang, S. D. Chao, and R. T. Skodje, Nature (London) **419**, 281 (2002); S. D. Chao, S. A. Harich, D. X. Dai, C. C. Wang, X. Yang, and R. T. Skodje, J. Chem. Phys. **117**, 8341 (2002).
[11] F. Fernández-Alonso, Ph.D. thesis, Stanford University, 1999.
[12] B. K. Kendrick, L. Jayasinghe, S. Moser, M. Auzinsh, and N. Shafer-Ray, Phys. Rev. Lett. **84**, 4325 (2000); B. K. Kendrick, L. Jayasinghe, S. Moser, M. Auzinsh, and N. Shafer-Ray, *ibid.* **86**, 2482 (2001).
[13] W. H. Miller and J. Z. H. Zhang, J. Phys. Chem. **95**, 12 (1991).
[14] F. J. Aoiz, V. J. Herrero, and V. Sáez Rábanos, J. Chem. Phys. **97**, 7423 (1992).
[15] R. T. Skodje, D. Skouteris, D. E. Manolopoulos, S.-H. Lee, F. Dong, and K. Liu, Phys. Rev. Lett. **85**, 1206 (2000); J. Chem. Phys. **112**, 4536 (2000); S. C. Althorpe, Chem. Phys. Lett. **370**, 443 (2003).
[16] S. C. Althorpe, F. Fernández-Alonso, B. D. Bean, J. D. Ayers, A. E. Pomerantz, R. N. Zare, and E. Wrede, Nature (London) **416**, 67 (2002).
[17] F. J. Aoiz, L. Bañares, J. F. Castillo, and D. Sokolvski, J. Chem. Phys. **117**, 2546 (2002).
[18] B. K. Kendrick, J. Chem. Phys. **114**, 8796 (2001).
[19] S. C. Althorpe, J. Chem. Phys. **117**, 4623 (2002).
[20] D. Sokolovski, Chem. Phys. Lett. **370**, 805 (2003).
[21] T. C. Allison, R. S. Friedman, D. J. Kaufman, and D. G. Truhlar, Chem. Phys. Lett. **327**, 439 (2000).
[22] N. E. Shafer, A. J. Orr-Ewing, W. R. Simpson, H. Xu, and R. N. Zare, Chem. Phys. Lett. **212**, 155 (1993).
[23] W. R. Simpson, A. J. Orr-Ewing, T. P. Rakitzis, S. A. Kandel, and R. N. Zare, J. Chem. Phys. **103**, 7299 (1995).
[24] P. M. Regan, S. R. Langford, A. J. Orr-Ewing, and M. N. R. Ashfold, J. Chem. Phys. **110**, 281 (1999).
[25] F. Fernández-Alonso, B. D. Bean, R. N. Zare, F. J. Aoiz, L. Bañares, and

J. F. Castillo, J. Chem. Phys. **115**, 4534 (2001).
[26] G. C. Bjorklund, C. P. Ausschnitt, R. R. Freeman, and R. H. Storz, Appl. Phys. Lett. **33**, 54 (1978).
[27] D. A. Dahl, SIMION 3D version 6.0 (U.S. Department of Energy, Office of Energy Research, Idaho Falls, Idaho, 1995).
[28] D. S. Zakheim and P. M. Johnson, Chem. Phys. **46**, 263 (1980).
[29] S. C. Althorpe (personal communication).
[30] S. Althorpe and D. Clary, Annu. Rev. Phys. Chem. **54**, 493 (2003).